

Ground state phase diagram of spin-1/2 bosons in a two-dimensional optical lattice

L. de Forges de Parny¹, F. Hébert¹, V.G. Rousseau², R.T. Scalettar³, and G.G. Batrouni^{1,4}

¹*INLN, Université de Nice-Sophia Antipolis, CNRS; 1361 route des Lucioles, 06560 Valbonne, France,*

²*Department of Physics and Astronomy, Louisiana State University, Baton Rouge, Louisiana 70803, USA,*

³*Physics Department, University of California, Davis, CA 95616, and*

⁴*Centre for Quantum Technologies, National University of Singapore; 2 Science Drive 3 Singapore 117542.*

We study a two-species bosonic Hubbard model on a two-dimensional square lattice by means of quantum Monte Carlo simulations. In addition to the usual contact repulsive interactions between the particles, the Hamiltonian has an interconversion term which allows the transformation of two particles from one species to the other. The phases are characterized by their solid or superfluid properties and by their polarization, *i.e.* the difference in the populations. When inter-species interactions are smaller than the intra-species ones, the system is unpolarized, whereas in the opposite case the system is unpolarized in even Mott insulator lobes and polarized in odd Mott lobes and also in the superfluid phase. We show that in the latter case the transition between the Mott insulator of total density two and the superfluid can be either of second or first order depending on the relative values of the interactions, whereas the transitions are continuous in all other cases.

PACS numbers: 05.30.Jp, 03.75.Hh, 67.40.Kh, 75.10.Jm 03.75.Mn

I. INTRODUCTION

Since their first experimental realization, atomic Bose-Einstein condensates have been used as a tool to study strongly interacting quantum systems. This made possible the study of exotic phases, especially in systems governed by Hamiltonians not easily realized in condensed matter. Soon after the initial work on spin-0 bosons [1], much effort was directed at the problem of mixtures of different kind of particles: fermions [2] or mixtures of bosons and fermions [3]. However, in these studies, the effective spin degrees of freedom are frozen and the number of particles of each type is generally fixed. Purely optical trapping techniques allow to trap the atoms without freezing the internal degrees of freedom. These systems exhibit both magnetic and superfluid properties offering the opportunity to study the interplay between these two effects. Unlike in simple mixtures, spin-spin interactions are present in these systems and can be either ferromagnetic (⁸⁷Rb) or antiferromagnetic (²³Na)[4, 5].

Whereas current spin-1 experiments are in continuous space, a simple model was proposed [6] for a system on an optical lattice with only two internal low energy states. The proposed system consider neutral polarizable atoms with three degenerate atomic ground states and three degenerate excited states characterized by the magnetic quantum number $S_z = 0, \pm 1$. In addition to generating a periodic (optical lattice) potential, the counter propagating lasers couple these internal ground and excited states by V and Λ transitions which leads to only two low energy eigenstates denoted respectively 0 and Λ . Such particles with only two internal effective degrees of freedom are referred to as spin-1/2 bosons. As in the spin-1 case, the interaction between these spins can be ferromagnetic or antiferromagnetic and the presence of an optical lattice allows the system to become strongly correlated with superfluid (SF) or Mott insulator (MI) phases. In previous work [7], we extended the original mean-field the-

ory (MFT) approach [6] and studied the one-dimensional system with exact quantum Monte Carlo (QMC) simulations. Related spin-1 models were considered using MFT [8, 9] or in one dimension using QMC [10]. A similar model with two species of bosons that can convert into each other was also studied [11].

If the spin-spin interactions for the original spin one bosons are ferromagnetic (F), the resulting on-site repulsions for spin 1/2 bosons are smaller between different particles than between identical particles [6, 7]. In that case MFT and QMC both show the system never polarizes [7]; in other words, the populations of the two species always remain equal. If the repulsion is strong enough, the system is in a Mott insulating phase for commensurate densities and is otherwise superfluid. The transitions between the superfluid and the Mott phases are always continuous.

In the case of antiferromagnetic (AF) interactions for the original spin one bosons, the repulsion between different particles is stronger than the repulsion between identical particles [6, 7] in the resulting spin 1/2 model and the system exhibits a richer phase diagram. First, the Mott phases are polarized for odd densities while they are unpolarized for even ones. In addition, the superfluid phase is always polarized. Finally, MFT predicts second order transitions between the odd density Mott phases and the superfluid whereas the transitions between even MI and SF can be first or second order depending on the strength of the interaction. This was not observed in the one dimensional QMC simulations [7]. This discrepancy was not surprising since MFT often fails in reduced dimensionality and also since first order phase transitions are generally absent in one dimension. Another feature of the AF regime is a phase transition between a polarized and an unpolarized phase inside the $\rho = 1$ (ρ being the total particles density) Mott phase at low temperature observed with the QMC simulations.

In this paper, we extend the QMC study of this sys-

tem to the two dimensional square lattice. The paper is organized as follows. In section II, we will review the model and the techniques used to study it. Sections III and IV will be devoted to the presentation of our results for the cases of larger repulsion between different or identical particles, respectively. We summarize these results in Section V.

II. SPIN-1/2 MODEL

The model we will study has two species of bosonic particles governed by the Hamiltonian [6],

$$\mathcal{H} = -t \sum_{\sigma, \langle \mathbf{r}, \mathbf{r}' \rangle} \left(a_{\sigma \mathbf{r}}^\dagger a_{\sigma \mathbf{r}'} + a_{\sigma \mathbf{r}'}^\dagger a_{\sigma \mathbf{r}} \right) - \mu \sum_{\sigma, \mathbf{r}} \hat{n}_{\sigma \mathbf{r}} \quad (1)$$

$$+ \frac{U_0}{2} \sum_{\sigma, \mathbf{r}} \hat{n}_{\sigma \mathbf{r}} (\hat{n}_{\sigma \mathbf{r}} - 1) + (U_0 + U_2) \sum_{\mathbf{r}} \hat{n}_{0 \mathbf{r}} \hat{n}_{\Lambda \mathbf{r}} \quad (2)$$

$$+ \frac{U_2}{2} \sum_{\mathbf{r}} \left(a_{0 \mathbf{r}}^\dagger a_{0 \mathbf{r}}^\dagger a_{\Lambda \mathbf{r}} a_{\Lambda \mathbf{r}} + a_{\Lambda \mathbf{r}}^\dagger a_{\Lambda \mathbf{r}}^\dagger a_{0 \mathbf{r}} a_{0 \mathbf{r}} \right), \quad (3)$$

where $a_{\sigma \mathbf{r}}^\dagger$ creates a particle of “spin” $\sigma = 0, \Lambda$ on site $\mathbf{r} = (x, y)$ of a periodic square lattice of size $L \times L$. The $\hat{n}_{\sigma \mathbf{r}} = a_{\sigma \mathbf{r}}^\dagger a_{\sigma \mathbf{r}}$ are the corresponding number operators counting the particles of type σ on site \mathbf{r} . The Hamiltonian includes the conventional hopping term (Eq. (1)) which plays the role of a kinetic energy term for lattice systems with the associated hopping parameter t that is used as the energy scale. To study the system in the grand canonical ensemble, a chemical potential term is added to the Hamiltonian (1). There are two density-density interaction terms (Eq. (2)). The first describes repulsion between identical particles on the same site with an associated energy $U_0 > 0$. The second describes the on-site repulsion between particles of different types. Depending on the value of U_2 , this repulsion can be stronger ($U_2 > 0$) or smaller ($U_2 < 0$) than the repulsion between identical particles. In this work, $|U_2|$ will remain smaller than U_0 in order to keep only repulsive interactions. In most of our work we kept U_2/U_0 fixed as U_0 is changed to map the phase diagram. Finally the last term of the Hamiltonian describes conversion between the species: As two identical particles collide on the same site, they can be converted into two particles of the other kind. It was shown in Ref. [6] that the matrix element for this conversion is equal to $U_2/2$, that is, it is essentially the difference of interaction energies between identical and different particles. The sign of the conversion term (Eq. (3)) can be chosen freely due to a symmetry of the model [7]. Here our convention has the opposite sign of the original paper [6].

The only term in the Hamiltonian that couples different sites is the hopping term in (1). MFT [6, 7] isolates one site \mathbf{r} and couples it to surrounding sites \mathbf{r}' via the mean values of destruction or creation operators $\psi_0 = \langle a_{0 \mathbf{r}'} \rangle = \langle a_{0 \mathbf{r}}^\dagger \rangle$ and $\psi_\Lambda = \langle a_{\Lambda \mathbf{r}'} \rangle = \langle a_{\Lambda \mathbf{r}}^\dagger \rangle$. This

results in a one-site Hamiltonian which can be easily diagonalized numerically. The ground state energy is then minimized with respect to the two mean-field order parameters ψ_0 and ψ_Λ . Normal or insulating phases are obtained when $\psi_0 = \psi_\Lambda = 0$ whereas superfluid phases occur whenever one of the ψ is non zero. To study this system exactly, we used the stochastic Green function (SGF) quantum Monte Carlo algorithm [12, 13]. This algorithm works in the canonical or grand canonical ensembles at finite inverse temperature $\beta = 1/kT$. We generally used $\beta = 2L/t$ which is usually a low enough temperature to obtain results that have converged to their ground state limit for a system of linear size L with moderate interactions. However (see below) for the strongly interacting regimes, it is sometimes necessary to use lower temperatures (up to $\beta = 4L/t$). In the canonical case with N particles, the chemical potential is defined as the discrete difference of the energy $\mu(N) = E(N+1) - E(N)$ which is valid in the ground state where the free energy is equal to the internal energy. The total particle density, ρ , is either fixed in the canonical case or fluctuates in the grand canonical one. Densities for particles of types 0 and Λ are called ρ_0 and ρ_Λ , respectively, and are not conserved due to the conversion term Eq. (3). The superfluid density is given by the fluctuations of the winding number [14]

$$\rho_s = \frac{\langle (W_0 + W_\Lambda)^2 \rangle}{4t\beta}. \quad (4)$$

As explained in Ref. [15], it is not meaningful to define individual superfluid densities for the 0 and Λ particles as their numbers are not conserved separately due to the conversion term Eq. (3). We also studied the single particle Green functions,

$$G_\sigma(\mathbf{R}) = \frac{1}{2L^2} \sum_{\mathbf{r}} \langle a_{\sigma \mathbf{r} + \mathbf{R}}^\dagger a_{\sigma \mathbf{r}} + a_{\sigma \mathbf{r}}^\dagger a_{\sigma \mathbf{r} + \mathbf{R}} \rangle, \quad (5)$$

where $\sigma = 0, \Lambda$. The Fourier transforms of the Green functions, Eq.(5), give the momentum distributions, $\rho_\sigma(\mathbf{k})$. The total density at zero momentum, $\rho(\mathbf{k} = 0)$, is given by

$$\rho(\mathbf{k} = 0) = \sum_{\sigma} \rho_\sigma(\mathbf{k} = 0). \quad (6)$$

Another useful quantity to characterize the Mott insulator is the two-particle anti-correlated Green function G_a

$$G_a(\mathbf{R}) = \frac{1}{2L^2} \sum_{\mathbf{r}} \left\langle a_{\Lambda \mathbf{r}}^\dagger a_{0 \mathbf{r} + \mathbf{R}}^\dagger a_{0 \mathbf{r}} a_{\Lambda \mathbf{r} + \mathbf{R}} + \text{H.c.} \right\rangle, \quad (7)$$

which is a measure of the exchange process whereby, for example, a 0 particle is annihilated at site \mathbf{r} and a Λ particle at site $\mathbf{r} + \mathbf{R}$ while a 0 particle is created at site $\mathbf{r} + \mathbf{R}$ and a Λ particle at site \mathbf{r} . If perfect phase coherence is established by means of particle exchange, G_a reaches its limiting upper value of $\rho_0 \rho_\Lambda$ at long distances \mathbf{R} .

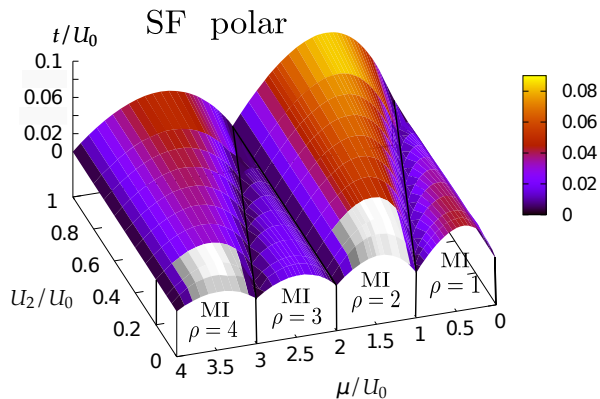


FIG. 1: (Color online) Zero temperature MFT phase diagram of the bosonic spin-1/2 model in the $U_2 > 0$ case. The dome-shaped surface shows the quantum phase transition between MI (below the surface) and SF regions (above). The grey areas indicate the regions where the transition is first order. Everywhere else the transitions are continuous. The transitions are also second order for $U_2 = 0$.

III. POSITIVE U_2 CASE

In the case where $U_2 > 0$, MFT predicts at zero temperature [7] that the system is either in a polarized superfluid (SF) phase or in incompressible Mott insulating (MI) phases. In the polarized superfluid phase, the symmetry between the two populations is broken and the density of one species becomes larger than the other. For total fillings which are odd multiples of the number of sites, *i.e.* $\rho = 1, 3 \dots$, the MI phases are also polarized whereas for even total densities, they are not: $\rho_0 = \rho_\Lambda$. The MI-SF transition is predicted to be continuous for odd density Mott phases. For even densities, the transition is found to be first order at the tip of the MI lobes for small U_2/U_0 and becomes continuous as U_2/U_0 increases (see Fig. 1). In the strongly interacting limit $t/U_0 \rightarrow 0$, the Mott phases of odd density ρ are found for chemical potentials μ in the interval $\rho - 1 < \mu/U_0 < \rho - U_2/U_0$, whereas the even density Mott phases are observed for $\rho - 1 - U_2/U_0 < \mu/U_0 < \rho$. Hence as observed in Fig. 1 or Fig. 2, the odd density Mott regions shrink as U_2/U_0 is increased and disappear for $U_2/U_0 = 1$ in this $t = 0$ limit.

Using QMC simulations in the one-dimensional case [7], we observed the polarized SF phase, the polarized MI lobes for $\rho = 1$ and the unpolarized MI for $\rho = 2$. However, contrary to MFT predictions, all transitions were continuous; as is often the case in one dimensional systems, no first order transitions were found. We also observed, at low temperature, that as t/U_0 decreases (always keeping U_2/U_0 constant) the $\rho = 1$ MI changes nature from polarized to unpolarized.

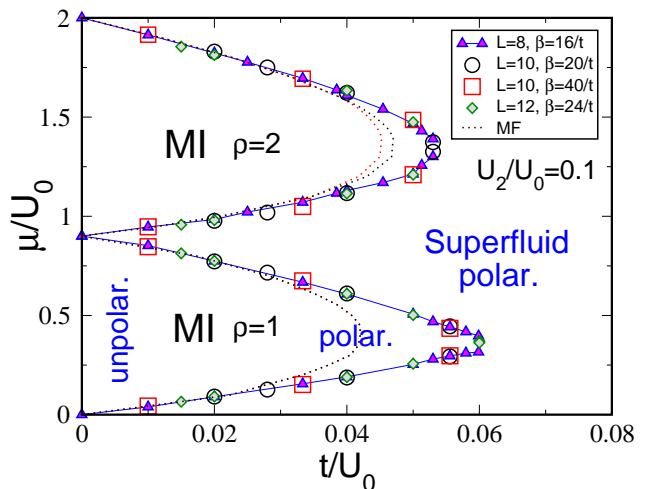


FIG. 2: (Color online) QMC phase diagram at $\beta = 2L/t$ or $4L/t$ for $U_2/U_0 = 0.1$ and several linear system sizes L . The superfluid phase is always polarised and the $\rho = 2$ MI is not polarized due to the effect of the interspecies exchange term. For the $\rho = 1$ MI phase, the system is polarized for the larger values of t/U_0 but then becomes unpolarized as t/U_0 decreases at finite $kT = t/2L$. As T decreases further to $kT = t/4L$ polarization appears (see Fig. 8). The dotted lines are the mean-field results. The region between the two MFT curves in the $\rho = 2$ lobe shows the coexistence zone due to the predicted first order transition.

A. Phase diagram

To map out the phase diagram, we employ the SGF algorithm in its canonical implementation. The chemical potential is calculated using energy differences to determine the boundaries of the MI lobes for $\rho = 1, 2$. In addition, we studied the histograms of the densities of the two species to determine whether a phase is polarized or not. We found results similar to those found in one dimension: The superfluid phase is always polarized, the $\rho = 2$ MI phase is not polarized and the $\rho = 1$ shows a transition between a polarized MI and an unpolarized MI as t/U_0 decreases. This point will be discussed in more detail in Sec. III C. The resulting phase diagram is shown in Fig. 2 for several linear lattice sizes, L , and $\beta = 1/kT = 2L/t$ or $\beta = 4L/t$.

The agreement between the QMC results and MFT is quite good. The Mott lobes obtained with MFT are shown as dotted lines in Fig. 2 and are close to the exact boundary for small values of t/U_0 with disagreement increasing as the tips of the lobes are approached due to increased quantum fluctuations. As expected, the agreement is much better than in one dimension where we had found a factor of two difference between the MFT predictions and the observed lobe tips.

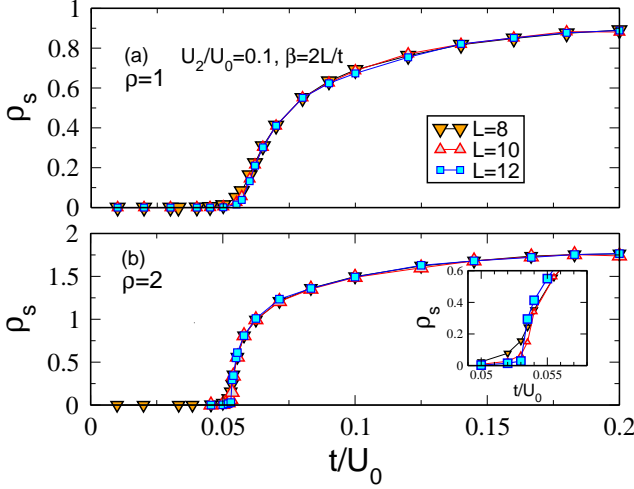


FIG. 3: The SF density, Eq. (4) as a function of t/U_0 at fixed total particle density for $U_2/U_0 = 0.1$. The transition from the MI (small t/U_0) to the SF phase is signaled by ρ_s becoming finite. For $\rho = 1$ (a) the transition is continuous whereas the jump in ρ_s marks the presence of a first order phase transition for $\rho = 2$ (b). See Figs. 4, 5, and 6. The inset shows the transition region and the jumps in more detail.

B. Phase transitions

An important difference between one and two dimensions is that first-order phase transitions may appear in the latter whereas they are essentially excluded in the former. Since MFT predicts a first order phase transition for even Mott lobes, we used QMC to study this transition in great detail.

Figure 3 shows the evolution of the superfluid density ρ_s at the MI-SF transition at fixed total density while varying t/U_0 , in other words the transition at the tip of the Mott lobe. We observe that in the $\rho = 1$ case (Fig. 3(a)), the transition is continuous. There is no evidence at all for a first order transition for this case. On the contrary, in the $\rho = 2$ case (Fig. 3(b)), a jump in the superfluid density indicates a first order phase transition.

Comparing this $\rho = 2$ case with MFT results for different values of U_2/U_0 in Fig. 4, we observe very similar behavior. The transition is continuous for $U_2/U_0 = 0$. Then it becomes discontinuous for small values of $U_2/U_0 \lesssim 0.25$ and is again continuous for $U_2/U_0 \geq 0.25$. The jump in the superfluid density varies continuously from zero at $U_2/U_0 = 0$ to a maximum for $U_2/U_0 \approx 0.05$ and then decreases back to zero as U_2/U_0 is increased further. Figure 5 shows similar behavior for the particle density at zero momentum, $\rho(\mathbf{k} = 0)$, where, once again, the jump at the transition is observed for small values of U_2/U_0 .

To confirm the presence of first order phase transitions near the tip of the MI lobe for even densities, we studied the behavior of ρ as a function of μ as one cuts across the lobe at fixed t/U_0 using QMC simulation in the canonical and grand canonical ensembles. In the canonical ensemble,

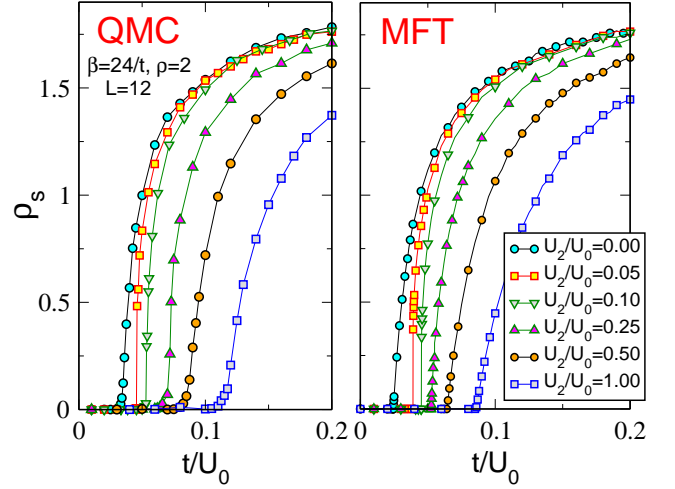


FIG. 4: (Color online) The superfluid density from QMC and MFT calculations as a function of t/U_0 for $\rho = 2$ and for several positive values of U_2/U_0 . Both methods exhibit a jump in ρ_s indicating the presence of a first order transition at the tip of the $\rho = 2$ Mott lobe for small but finite values of U_2/U_0 . The jumps increases from 0 at $U_2/U_0 = 0$ to a maximum for $U_2/U_0 \approx 0.05$ and then decreases back to zero for $U_2/U_0 \geq 0.25$.

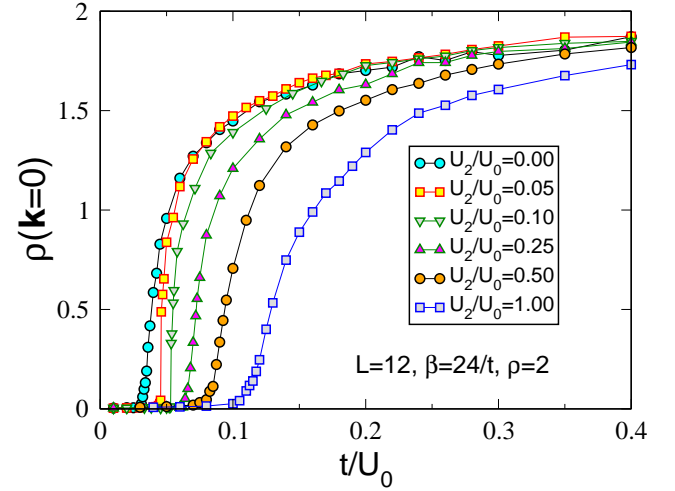


FIG. 5: (Color online) The density in the $\mathbf{k} = 0$ momentum $\rho(\mathbf{k} = 0)$ as a function of t/U_0 for $\rho = 2$ and for several values of U_2/U_0 . As for ρ_s , Fig. 4, we observe a jump in $\rho(\mathbf{k} = 0)$ for small but finite values of U_2/U_0 , confirming the presence of a first order transition.

ble, a first order transition is signaled by negative compressibility [16], $\kappa \propto \partial\rho/\partial\mu < 0$. In the grand canonical ensemble, there will be a corresponding discontinuous jump in the ρ versus μ curve. Figure 6 shows both these cases. In Fig. 6(a) the canonical simulations clearly show negative κ just before and after the Mott plateau at $\rho = 2$. On the other hand, the grand canonical ensemble, Fig. 6(b), shows discontinuous jumps in ρ at the corresponding values of μ . The canonical and grand canonical

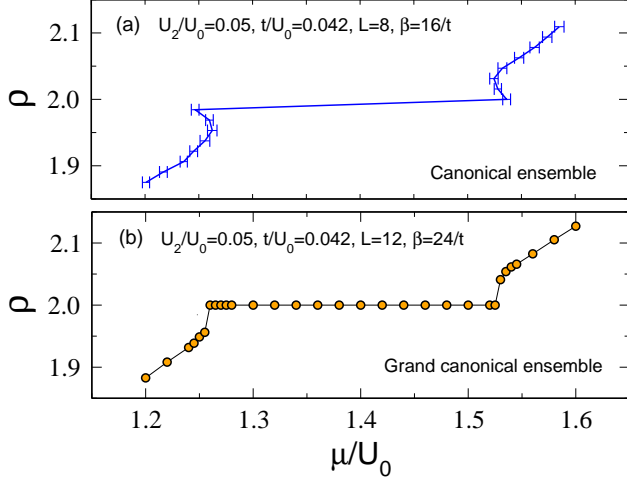


FIG. 6: (Color online) The density, ρ , as a function of the chemical potential, μ , close to the tip of the $\rho = 2$ Mott lobe. The canonical simulation (a) shows a negative compressibility region, $\kappa \propto \partial\rho/\partial\mu < 0$. The grand canonical simulation (b) exhibits a corresponding jump in the density. Thus both approaches show the presence of a first order transition.

simulations are in quantitative agreement on the size of the unstable region which is extremely narrow; the system is stable for densities smaller than $\rho = 1.95$ or larger than $\rho = 2.05$ for the chosen value of t/U_0 .

C. Polarization and nature of the Mott phases

We now analyse in more detail the polarization properties of the Mott phases. In the $\rho = 1$ MI phase, Fig. 7 shows that a transition between unpolarized and polarized regions occurs for $t/U_0 \simeq 0.02$ for $L = 8$ and $\beta = 2L/t$. This is well inside the MI region as can be seen from the phase diagram, Fig. 2. This possibility of a polarization transition deep in the MI lobe requires closer examination.

In the $\rho = 1$ MI phase, the system is frozen in a state with one particle per site. Fluctuations around this state will occur when particles hop around. However, events where two particles are converted to the other species are negligible since this requires double occupancies. Neglecting conversions and taking the hopping term as perturbation to second order, the model can then be mapped onto an anisotropic Heisenberg model [17] where the presence of a Λ particle on a site corresponds to an up spin along the z axis and a 0 particle corresponds to a down spin. The interactions between spins in the xy plane and along the z direction are given by [17]

$$\begin{aligned} J_{xy} &= -\frac{2t^2}{U_0} \frac{1}{1 + U_2/U_0} \\ J_z &= -\frac{2t^2}{U_0} \frac{1 + 2U_2/U_0}{1 + U_2/U_0} \end{aligned} \quad (8)$$

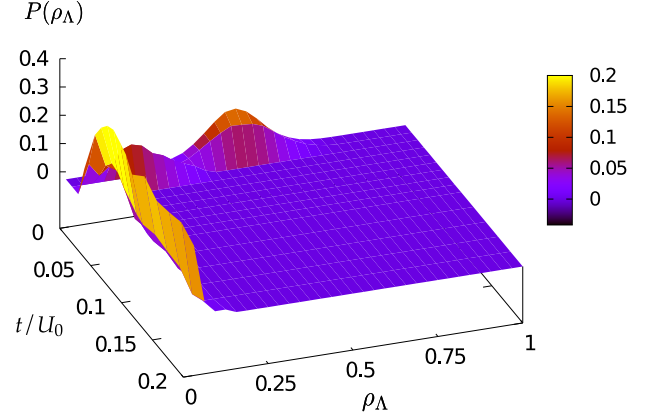


FIG. 7: (Color online) Histogram of the density of Λ particles for $U_2 > 0$ as a function of t/U_0 . The total density is fixed at $\rho = 1$ and the histogram of the 0 particles is the image of this distribution with respect to the line $\rho_\Lambda = 0.5$. The other parameters are $L = 8$, $\beta = 2L/t$, and $U_2/U_0 = 0.1$. The system polarizes for $t/U_0 \simeq 0.02$, well inside the $\rho = 1$ Mott lobe. Thus at this low, albeit finite, temperature, there is a transition between a polarized Mott phase at large t/U_0 and an unpolarized Mott phase at lower t/U_0 . As shown in Fig. 8 the complete lobe is polarized at $T = 0$.

For $U_2 > 0$, we see that the couplings J_{xy} and J_z are always negative, *i.e.* the effective model spin interactions are always ferromagnetic. We also see that $|J_z| > |J_{xy}|$, which means that ferromagnetic order will develop along the z direction. In other words, the system will become polarized in terms of 0 or Λ particles in the ground state limit.

However, we also see that the energy associated with the polarization of the system is t^2/U_0 and becomes very small in the large U_0 limit. On the other hand, the histogram in Fig. 7 is at fixed temperature, $\beta = 2L/t$, which means that the system is no longer in the zero temperature limit for small values of $t/U_0 \leq 0.02$ for $L = 8$. Then excitations of these spin degrees of freedom occur and the system is no longer polarized.

This argument is confirmed by QMC simulations done at lower temperature: In Fig. 8 we show the evolution of the histogram of ρ_Λ for given values of U_0 and U_2 and for several inverse temperatures from $\beta = 2L/t$ to $\beta = 4L/t$. We observe that as the temperature is decreased, the system polarizes. We then conclude that, in the ground state limit, the entire $\rho = 1$ Mott phase is polarized, although one needs extremely low temperatures in order to observe the polarization for large U_0 .

Figure 9 shows single particle and anticorrelated Green functions in the MI (a) and SF (b) phases. As expected, we see in the Mott phase, Fig. 9(a), that the individual Green functions G_0 and G_Λ decay exponentially to zero with distance. The Heisenberg model approach predicts that, besides the polarization of the system, ferromagnetic correlations in the xy plane should be present. In

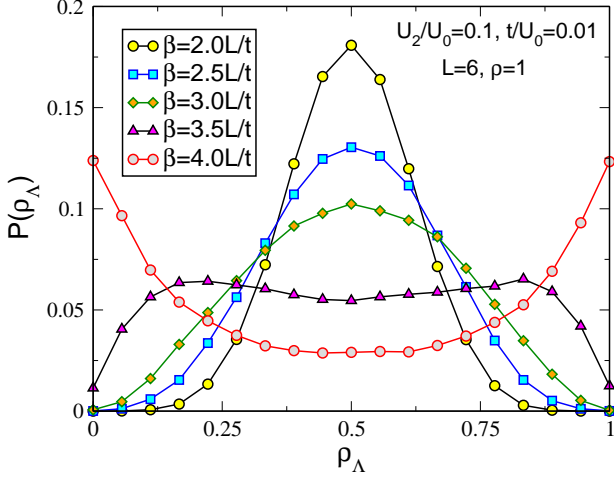


FIG. 8: (Color online) Histogram of the density of the Λ particles as a function of temperature. For large values of U_0 , one needs very small temperature for the system to polarize as the energy associated to the polarization decreases when U_0 increases.

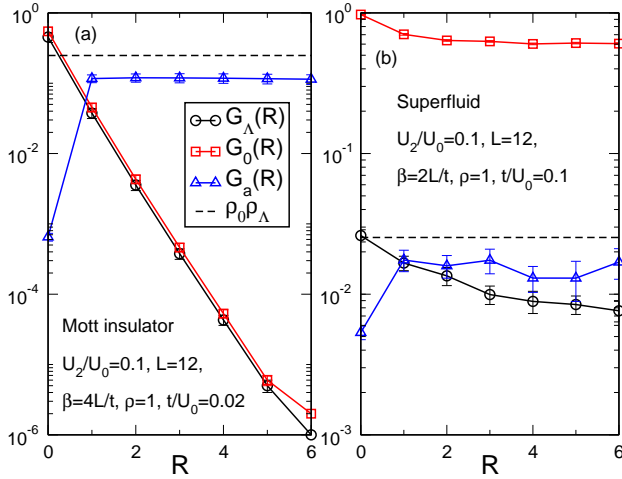


FIG. 9: (Color online) The single particle and the anticorrelated Green functions for $U_2 > 0$ and $\rho = 1$ along the x axis in the Mott insulator (a) and superfluid phases (b). In the MI phase, individual movements of particles are strongly suppressed as shown by the exponential decay of G_0 and G_Λ whereas some anticorrelated movements of particles remain, which is shown by the plateau in G_a . In the superfluid phase, we find a long range order for the Green function corresponding to the dominant species 0.

the xy plane spin-spin correlations are measured with the correlation function $\langle S_{x,\mathbf{r}+\mathbf{R}} S_{x,\mathbf{r}} + S_{y,\mathbf{r}+\mathbf{R}} S_{y,\mathbf{r}} \rangle$ which, in terms of the particle creation and annihilation operators, maps into the anticorrelated Green function G_a , Eq. 7. In a system where the density is fixed to one particle per site due to interactions but where there are different species, there is always the possibility that particles move by exchanging their positions. G_a measures the co-

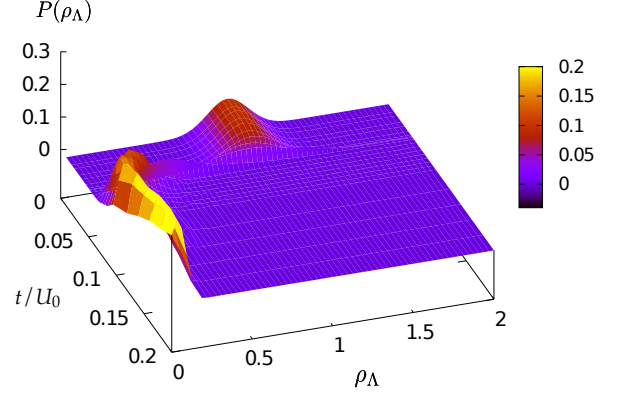


FIG. 10: (Color online) Histogram of the density of Λ particles for $U_2 > 0$ as a function of t/U_0 at fixed total density, $\rho = 2$. The histogram of the 0 particles is the image of this distribution with respect to the line $\rho = 1$. The other parameters are $L = 8$, $\beta = 2L/t$, $U_2/U_0 = 0.1$. The system polarizes for $t/U_0 \simeq 0.05$ which corresponds to the MI-SF transition. Hence the $\rho = 2$ Mott is unpolarized.

herence at long range of such exchange moves. Indeed we see that such exchanges are present in the $\rho = 1$ Mott phase because G_a stays almost constant as distance is increased, although it is smaller than its limiting value $\rho_0 \rho_\Lambda$. This supports the description of the system, at strong coupling, in terms of Heisenberg spins since individual particle degrees of freedom appear to be irrelevant to the excitations present in the system. On the other hand, spin excitations (*i.e.* exchanges of particles) appear to be relevant.

In the superfluid phase, the Green function of the dominant species (0 in the case shown in Fig. 9 (b)) shows long range order, indicating the presence of a long range phase coherence. We also observe long range coherence for the minority species and for the anticorrelated Green function. This is typical of a strongly correlated superfluid where different kinds of phase coherence can be observed: Phase coherence of the individual particles, but also, at the same time, phase coherence of exchange moves of particles.

In the $\rho = 2$ MI case, the situation is simpler since the phase is not polarized. With positive U_2 , the system will adopt a state where there are two particles of the same type on a given site. However, the conversion term will couple this state with the corresponding state with two particles of the other kind on the site, thus lowering the energy. On average, those two states have the same probability, and the mean number of a given type of particle on a site is one. There is also no particular density ordering of the system. This behavior is illustrated in Fig. 10 where the histogram of ρ_Λ as a function of t/U_0 is shown. We see that the transition between the unpolarized phase at low t/U_0 and the polarized phase happens for $t/U_0 \simeq 0.05$. Comparing this with the phase

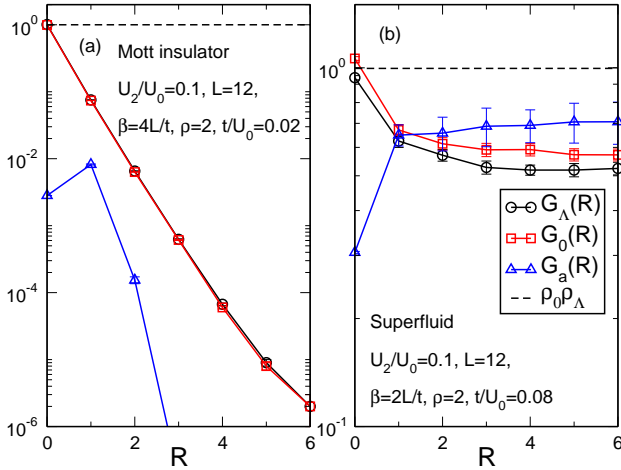


FIG. 11: (Color online) The single particle and the anticorrelated Green functions for $U_2 > 0$ and $\rho = 2$ along the x axis in the Mott (a) and superfluid phases (b). In the MI phase, individual movements as well as exchanges of particles are suppressed, which is shown by the exponential decay of all the Green functions. Phase coherence is established in the SF phase (b).

diagram Fig. 2, we find that the polarization occurs precisely at the MI-SF transition. Hence the $\rho = 2$ MI phase is not polarized but the superfluid phase is.

Neglecting the hopping term, there is no degeneracy in the state adopted by the system in the $\rho = 2$ Mott phase. Then the fluctuations induced by the hopping term do not create any phase coherence and all the Green functions decay exponentially (Fig. 11(a)). In the superfluid phase (Fig. 11(b)), we observe a behavior similar to the $\rho = 1$ case where all the Green functions reach a plateau at large distance, thus showing the presence of different kinds of phase coherence in the system. Due to the larger density and the importance of conversion processes in this case, the polarization of the system is weaker than in the $\rho = 1$ case and the leading phenomenon seems to be exchanges as G_a is larger than G_0 or G_Λ .

IV. NEGATIVE U_2 CASE

In the negative U_2 case, the phase diagram predicted by MFT, and observed in one-dimensional QMC simulations is less rich than its positive counterpart. As discussed in Section II, we focus on the range of interactions $|U_2|/U_0 < 1$. Figure 12 shows the MFT phase diagram which exhibits MI and SF phases, both of which are unpolarized. As $U_2/U_0 \rightarrow -1$ and for $t/U_0 = 0$, all the MI lobes, with even or odd densities, shrink and totally disappear at $U_2/U_0 = -1$ as the MI phase of density ρ is obtained for $(1 + U_2/U_0)(\rho - 1) < \mu/U_0 < (1 + U_2/U_0)\rho$. MFT predicts that all phases are unpolarized and all transitions continuous. This was confirmed in one di-

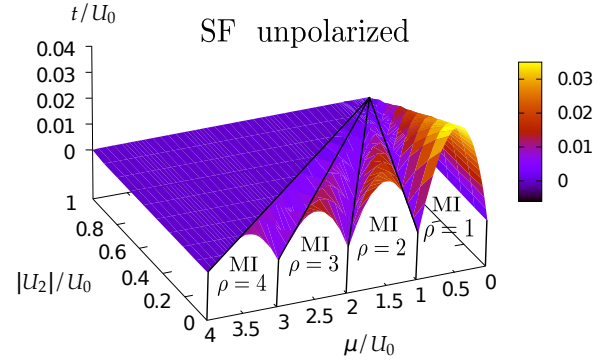


FIG. 12: (Color online) Ground state phase diagram of the $U_2 < 0$ case in MFT for $\rho \leq 4$. The surface traces the transition points between MI phases (below the surface) and SF regions (above). As $|U_2|/U_0 \rightarrow 1$, the MI regions shrink and eventually disappear.

mension with QMC simulations. Here, we focus on the two dimensional case.

A. Phase diagram and transitions

Fig. 13 shows the QMC phase diagram for the negative U_2 case at $U_2/U_0 = -0.1$. The boundaries of the MI lobes are obtained in the same way as in the positive U_2 case. The results are qualitatively similar to those found in one dimension. The system exhibits MI lobes at commensurate fillings and sufficiently small t/U_0 which turn superfluid as this parameter increases. In addition the system is SF for all incommensurate fillings. We find that both these phases are always unpolarized (see below). As for $U_2 > 0$, the agreement between QMC and MFT is better in two dimensions than in one, especially at small t/U_0 . The agreement is poor as the tips of the lobes are approached due to increased quantum fluctuations.

In contrast with the $U_2 > 0$ case, all quantum phase transitions appear to be continuous in this case. As can be observed in Fig. 14, there are no signs of possible discontinuities in the superfluid density at the transition between the MI and SF phases. Other quantities, such as $\rho(\mathbf{k} = 0)$ (not shown here) confirm this conclusion.

B. Polarization and nature of the Mott phases

To analyse the situation in the $\rho = 1$ MI, we again use the perturbative mapping to the anisotropic Heisenberg model (Eq. 8). We restrict ourselves to the case where all the interactions are repulsive: $-1 < U_2/U_0 < 0$. In this range $|J_{xy}| > |J_z|$ and the system develops spin ordering in the xy plane. In terms of the original model representing two types of particles, this spin order in the xy plane corresponds to a phase with equal number of

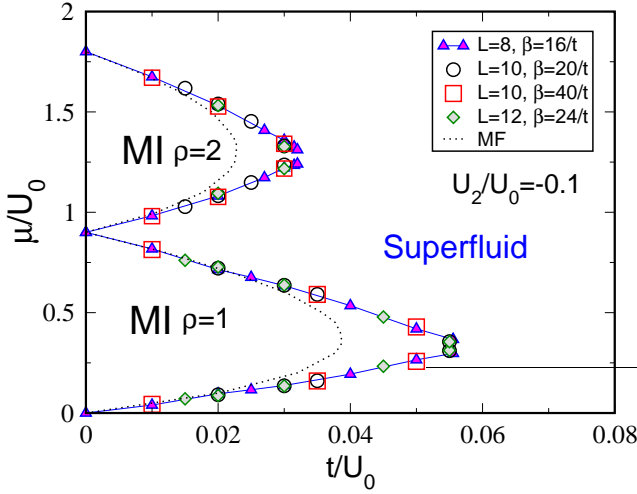


FIG. 13: (Color online) QMC phase diagram at low temperature for three system sizes in the $U_2 < 0$ case. Unlike the $U_2 > 0$ case, the system never polarizes. The dotted lines show the MFT result.

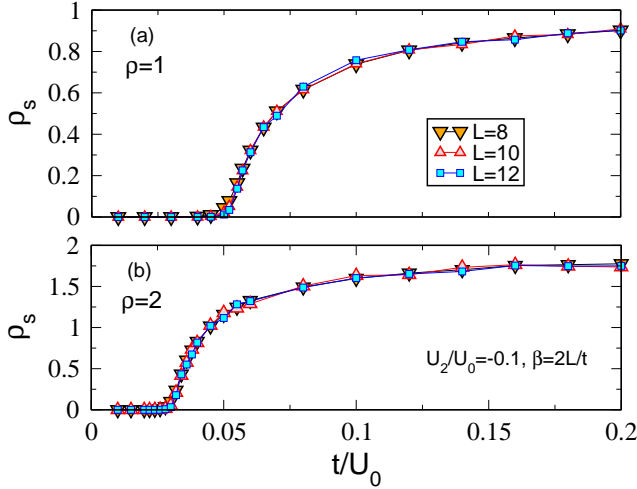


FIG. 14: (Color online) The SF density, ρ_s , as a function of t/U_0 at fixed density for $U_2 < 0$. The superfluid density varies continuously for $\rho = 1$ (a) and $\rho = 2$ (b), showing no sign of a first order phase transition.

0 and Λ particles on each site. This is confirmed by QMC simulations. Plotting the density histograms for $U_2/U_0 = -0.1$, Fig. 15, it is seen that the distribution is always centered around $\rho_0 = \rho_\Lambda = 0.5$ confirming that the system is not polarized. In addition, the density-density correlations (not shown) do not exhibit any sign of density order.

In this case, the prediction of the mapping onto the Heisenberg model is that the system should develop ferromagnetic order in the xy plane and the spin-spin correlations $\langle S_{x,\mathbf{r}+\mathbf{R}} S_{x,\mathbf{r}} + S_{y,\mathbf{r}+\mathbf{R}} S_{y,\mathbf{r}} \rangle$ should be long ranged. Figure 16 shows the single particle and the anticorrelated Green functions in the MI (a) and the SF (b) phases. In

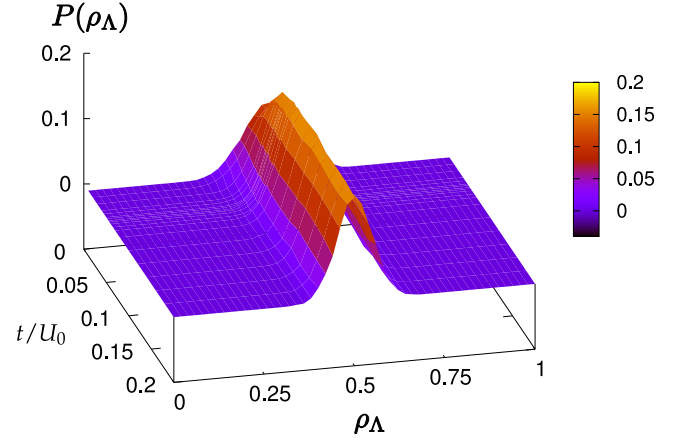


FIG. 15: (Color online) Histogram of the density for particles of type Λ for $U_2 > 0$ for a total density $\rho = 1$ and $U_2/U_0 = -0.1$, $L = 10$ and $\beta = 2L/t$. The histogram is always centered around $\rho_0 = \rho_\Lambda = 0.5$ and the system never becomes polarized in this case. There is no change of behavior when the MI-SF transition is crossed for $t/U_0 \simeq 0.05$.

the $\rho = 1$ MI phase, Fig. 16(a), we see that $G_0(\mathbf{R})$ and $G_\Lambda(\mathbf{R})$ decay exponentially as expected. However, we also see that $G_a(\mathbf{R})$ quickly saturates to a constant value at large separations indicating that exchange moves are common. In a system where the number of particles of each species is fixed, *i.e.* no conversion between species, this behavior of $G_a(\mathbf{R})$ would correspond to a counter superfluid phase (CSF) [17]. However, in this system, due to the residual effects of the conversion term, it is not possible to calculate a corresponding counter superfluid density [15]. However, we do observe the presence of a long range coherence of exchange moves as predicted by the perturbative mapping to the Heisenberg spin system. The plateau observed in G_a takes on its maximum possible value at large distances $G_a \rightarrow \rho_0 \rho_\Lambda$, showing perfect phase coherence, contrary to what was observed for $U_2 > 0$.

In the superfluid phase at $\rho = 1$, Fig. 16 (b), G_0 and G_Λ exhibit long range order, indicating the presence of phase coherence. The two species remain correlated, of course, since the system is still in a strongly interacting regime ($t/U_0 = 0.1$). This correlation can be observed, for example, from the fact that G_a is larger than the product $G_0 G_\Lambda$. This means that, while particles can move independently, exchanges of different particles are still present.

The $\rho = 2$ Mott phase is once again unpolarized (the histogram is similar to the $\rho = 1$ histogram shown in Fig. 15). In the $t/U_0 \rightarrow 0$ limit, there exist two possible degenerate ground states on each site. The first state is obtained by putting one particle of each type on a given site, thus obtaining an interaction energy $U_0 + U_2 < U_0$ as $U_2 < 0$. The second state is the superposition of a state with two 0 particles and a state with two Λ particles: $(|00\rangle + |\Lambda\Lambda\rangle)/\sqrt{2}$. While the interaction terms Eq. 2 gives in this case an energy U_0 , it is reduced to $U_0 + U_2$ by

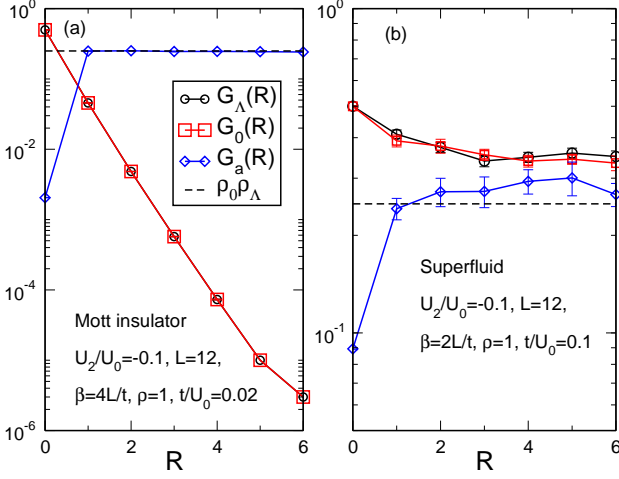


FIG. 16: (Color online) The single particle and anticorrelated Green functions for $U_2 > 0$ and $\rho = 1$ along the x axis in the MI (a) and SF phases (b). For the MI phase, as predicted by the spin approximation, we find a dominant G_a showing that the displacement of particles is due mainly to exchange of particles of different types whereas movements of individual particles are suppressed. For the superfluid phase, there is long range coherence of all the Green functions.

the conversion term Eq. 3. For these two possible states, the mean densities ρ_0 and ρ_Λ are equal and the system does not polarize which is directly observed in density histograms (not shown here). The $\rho = 2$ Mott ground state then shows a large degeneracy in the $t = 0$ on-site limit. All these degenerate states are once again coupled by second order contributions from the hopping term and the degeneracy is lifted by establishing a phase coherence of exchange movements. This can be understood in the following way: whether a site is occupied by two 0 particles, two Λ particles or one 0 and one Λ particle, the on site energy is the same, because the interaction energy is lower for different particles or because it is lowered by conversion term for identical particles. Then starting from any configuration, exchanges of particles of different types will exchange the states of neighboring sites without changing the on site energy. A phase coherence is then established by exchange moves in the Mott phase, reminiscent of the one observed in the $\rho = 1$ case. This is shown in Fig. 17(a) where we show perfect phase coherence of the G_a function which reaches its limiting value of $\rho_0 \rho_\Lambda = 1$ in the Mott phase whereas individual Green functions decay exponentially.

In the superfluid phase, we observe phase coherence both for exchange moves and for individual movements of particles but, once again, the exchange moves appear to give the leading contribution (Fig. 17(b)).

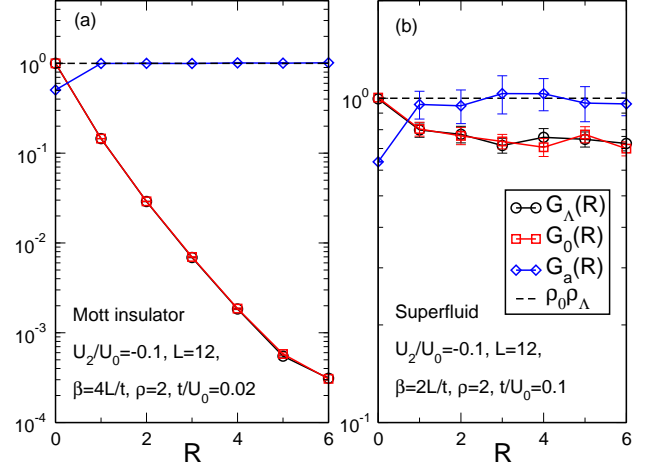


FIG. 17: (Color online) The single particle and anticorrelated Green functions for $U_2 < 0$ and $\rho = 2$ along the x axis in the MI (a) and SF phases (b). For the MI phase, there are exchanges of particles due to the degeneracy of the Mott phase in the $t = 0$ limit, whereas individual movements are prohibited. In the SF, all Green functions show phase coherence of individual movements of particles or of anticorrelated movements.

V. CONCLUSION

In this work, we used QMC simulations to determine the phase diagram of the spin-1/2 bosonic Hubbard model on a two-dimensional square lattice. For $U_2 > 0$, we found that the numerical results to be in good agreement with MFT, especially at very small t/U_0 where quantum fluctuations are highly suppressed. The system has three phases: A polarized superfluid, an unpolarized Mott phase for $\rho = 2$ (and likely for all even MI lobes) and a polarized Mott phase for $\rho = 1$ (and likely for all odd MI lobes). We have shown that the polarization of this $\rho = 1$ Mott phase can be understood in terms of an effective anisotropic Heisenberg model and that, in the ground state, the phase is completely polarized, although extremely low temperatures are needed to observe the polarization in the strongly interacting regime. The $\rho = 2$ phase is not polarized due to the action of the conversion term that will transform pairs of identical particles into pairs of the other types of particles and then suppress possible polarization of the system. The first order MI-SF transition for the $\rho = 2$ MI phase which was predicted by MFT is confirmed numerically. In addition, the QMC results showed that in the $\rho = 1$ MI lobe, moves which exchange the positions of a 0 and a Λ particles are present as evidenced by the saturation of the anticorrelated Green function G_a . This property was not previously addressed by MFT calculations.

For $U_2 < 0$, the system is always unpolarized and MI-SF transitions are all continuous. However, in the MI phases, the origin of this absence of polarization is differ-

ent for the $\rho = 1$ and the $\rho = 2$ phases. For $\rho = 1$, the anisotropic Heisenberg model approach shows the domination of an effective in-plane coupling, whereas for $\rho = 2$, the two possible degenerate states on each site are both unpolarized. Here too, we found that particle exchange moves are present in the $\rho = 1$ and, more surprisingly, in the $\rho = 2$ Mott insulator.

Acknowledgments

This work was supported by: the CNRS-UC Davis EPOCAL LIA joint research grant; by NSF grant OISE-0952300; an ARO Award W911NF0710576 with funds from the DARPA OLE Program.

-
- [1] M. Greiner, O. Mandel, T. Esslinger, T.W. Hänsch, and I. Bloch, *Nature* **415**, 39 (2002).
 - [2] M. W. Zwierlein, A. Schirotzek, C.H. Schunck, and W. Ketterle, *Science* **311**, 492 (2006); Y. Shin, C.H. Schunck, A. Schirotzek, and W. Ketterle, *Nature* **451**, 689 (2008).
 - [3] Y. Shin, A. Schirotzek, C.H. Schunck, and W. Ketterle, *Phys. Rev. Lett.* **101**, 070404 (2008).
 - [4] M. Vengalattore, S.R. Leslie, J. Guzman, and D.M. Stamper-Kurn, *Phys. Rev. Lett.* **100**, 170403 (2008); M. Vengalattore, J. Guzman, S. Leslie, F. Serwane, and D.M. Stamper-Kurn, *Phys. Rev. A* **81**, 053612 (2010).
 - [5] D.M. Stamper-Kurn and W. Ketterle, in *Coherent Atomic Matter Waves*, edited by R. Kaiser, C. Westbrook, and F. David, Springer, p. 137 (2001).
 - [6] K.V. Krutitsky and R. Graham, *Phys. Rev. A* **70**, 063610 (2004); K.V. Krutitsky, M. Timmer and R. Graham, *Phys. Rev. A* **71**, 033623 (2005).
 - [7] L. de Forges de Parny, M. Traynard, F. Hébert, V.G. Rousseau, R.T. Scalettar, and G.G. Batrouni, *Phys. Rev. A* **82**, 063602 (2010).
 - [8] V. Pai, K. Sheshadri, and R. Pandit, *Phys. Rev. B* **77**, 014503 (2008).
 - [9] T. Kimura, S. Tsuchiya, and S. Kurihara, *Phys. Rev. Lett.* **94**, 110403 (2005).
 - [10] G.G. Batrouni, V.G. Rousseau, and R.T. Scalettar, *Phys. Rev. Lett.* **102**, 140402 (2009).
 - [11] S. Takayoshi, M. Sato, and S. Furukawa, *Phys. Rev. A* **81**, 053606 (2010).
 - [12] V.G. Rousseau, *Phys. Rev. E* **77**, 056705 (2008).
 - [13] V.G. Rousseau, *Phys. Rev. E* **78**, 056707 (2008).
 - [14] D.M. Ceperley and E.L. Pollock, *Phys. Rev. B* **39**, 2084 (1984).
 - [15] M. Eckholt and T. Roscilde, *Phys. Rev. Lett.* **105**, 199603 (2010).
 - [16] G. G. Batrouni and R. T. Scalettar, *Phys. Rev. Lett.* **84**, 1599 (2000).
 - [17] A. B. Kuklov and B. Svistunov, *Phys. Rev. Lett.* **90**, 100401 (2003).